

Article

Kappa Carbide Precipitation in Duplex Fe-Al-Mn-Ni-C Low-Density Steel

Jaka Burja ^{1,2}, Barbara Šetina Batič ¹ and Tilen Balaško ^{2,*} 

¹ Institute of Metals and Technology, University of Ljubljana, 1000 Ljubljana, Slovenia; jaka.burja@imt.si (J.B.); barbara.setina@imt.si (B.Š.B.)

² Faculty of Natural Sciences and Engineering, University of Ljubljana, 1000 Ljubljana, Slovenia

* Correspondence: tilen.balasko@ntf.uni-lj.si; Tel.: +386-12000457

Abstract: The microstructural evolution of a Fe-Mn-Al-Ni-C low-density steel was studied. The lightweight low-density steels are a promising material for the transportation industry, due to their good mechanical properties and low density. The base microstructure of the investigated steel consists of ferrite and austenite. Thermo-Calc calculations showed the formation of an ordered BCC (body-centred cubic) B2 phase below 1181 °C and kappa carbides below 864 °C. The steel was produced in a vacuum induction furnace, cast into ingots and hot forged into bars. The forged bars were solution annealed and then isothermally annealed at 350, 450, 550, 650, 750, and 850 °C. The microstructure of the as-cast state, the hot forged state, solution annealed, and isothermally annealed were investigated by optical microscopy and scanning electron microscopy. The results showed the formation of kappa carbides and the ordered B2 phase. The kappa carbides appeared in the as-cast sample and at the grain boundaries of the isothermally annealed samples. At 550 °C, the kappa carbides began to form in the austenite phase and coarsened with increasing temperature.

Keywords: duplex steel; low-density steel; precipitation; kappa carbides



Citation: Burja, J.; Šetina Batič, B.; Balaško, T. Kappa Carbide Precipitation in Duplex Fe-Al-Mn-Ni-C Low-Density Steel. *Crystals* **2021**, *11*, 1261. <https://doi.org/10.3390/cryst11101261>

Academic Editor: José L. García

Received: 24 September 2021

Accepted: 17 October 2021

Published: 18 October 2021

Publisher's Note: MDPI stays neutral with regard to jurisdictional claims in published maps and institutional affiliations.



Copyright: © 2021 by the authors. Licensee MDPI, Basel, Switzerland. This article is an open access article distributed under the terms and conditions of the Creative Commons Attribution (CC BY) license (<https://creativecommons.org/licenses/by/4.0/>).

1. Introduction

Low-density steels have attracted increasing interest over the last decade, mainly due to the automotive industry's need for lighter materials with improved mechanical properties. Compared to conventional steels, low-density aluminium steels can achieve up to 20% reduction in density while exhibiting excellent mechanical properties such as yield strength, tensile strength, and elongation [1–12].

Low-density steels can be generally classified into ferritic, austenitic, and duplex steels based on their matrix phase microstructure, depending on the amount and type of alloying elements [1,3]. In addition to the matrix phase, these steels also contain κ -carbides, which are important for strain hardening of the steel, β -Mn, which is brittle and forms at a high Mn content, and intermetallic ordered precipitates [13–17].

In this work, we focused on the formation of the microstructure of a duplex low-density steel containing 10 wt.% Al, 14.8 wt.% Mn, and 5.6 wt.% Ni. We used optical microscopy (OM) and scanning electron microscopy (SEM) in combination with electron backscatter diffraction (EBSD) to observe the phases, crystal orientation, and orientation relationships. We observed the precipitation of the kappa-carbide phase in the austenite and the ferrite grains, with a well-defined orientation relationship between the parent and precipitated phase. Kappa carbides form in steels with high Mn and Al content. They have a primitive cubic unit cell that can be described as $(\text{Fe,Mn})_3\text{AlC}$. The precipitation of kappa carbides is essential for the design and understanding of the thermal treatment of low-density steels. Precipitation of the kappa-carbide phase occurs in the austenitic phase and increases the complexity of the microstructure. Precipitation of large coarse carbides or continuous strains of kappa carbides can be detrimental to mechanical properties [18,19].

However, the formation of the nano-sized kappa-carbide phase significantly improves the mechanical properties [15].

2. Materials and Methods

Ten kilograms of steel were melted in a vacuum induction melting furnace under a protective 300 mbar argon atmosphere. Pure elements, Al, Mn, Ni, C, and mild steel were used to produce the steel. The steel was cast into a 210 mm long ingot, which was 80 mm wide at the bottom and 90 mm wide at the top. The head of the ingot was cut of 40 mm from the top, to eliminate the shrinkage porosity. A sample for microstructural investigations was taken from the head of the ingot approximately 40 mm below the top and at $\frac{1}{4}$ of the outer diameter.

Chemical composition (Table 1) was measured by wet chemical analysis and infrared absorption after combustion ELTRACS-750 (ELTRA GmbH, Haan, Germany). The ingots were homogenized at 1200 °C for 30 min and hot forged to 40 mm × 40 mm. A sample was taken 30 mm from the forged bar, from the top of the ingot. The hot forged samples were solution annealed at 1200 °C and quenched in water, with one sample taken from the bar. The bar was cut into 30 mm pieces, which were then isothermally annealed at different temperatures (350, 450, 550, 650, 750, and 850 °C) for 2 h. The samples were then prepared for metallographic analysis by grinding and polishing. For microstructural observations, the samples were etched in 10% nital and for electron backscattered diffraction measurements the polished samples were additionally polished for 5 min using OPS (Oxide Polishing Suspension).

Table 1. Chemical composition of the sample.

C	Si	Cu	Ni	Mn	Al	Fe
0.82	0.2	0.17	5.6	14.8	10.0	balance

The chemical composition of the samples is given in Table 1.

Microstructural characterization was performed by optical microscopy and scanning electron microscopy JEOL JSM 6450-F (Jeol, Tokyo, Japan). Additional microanalysis was performed using energy dispersive spectroscopy (EDS) (Ultim®Max, Oxford Instruments, Abingdon, UK) and electron backscatter diffraction (EBSD) (EDAX, Mahwah, NJ, USA).

For CALPHAD predictions, we used the commercial software Thermo-Calc version 2021b (Thermo-Calc Software AB, Stockholm, Sweden) [20]. We chose the Thermo-Calc Software TCFE10 Steels/Fe-alloys database from which to obtain the thermodynamic data for the calculations [21]. We used Equilibrium Calculator and chose the calculation type Property Diagram, from which we obtained diagrams, showing the characteristic temperatures and the amount of thermodynamically stable phases in the studied steel.

3. Results and Discussion

3.1. Thermo-Calc Calculations

The Thermo-Calc calculations (Figure 1) showed that the solidification will contain ferrite and austenite. The calculated liquidus and solidus temperatures are 1392 and 1258 °C, respectively. The δ -ferrite (BCC_A2) begins to solidify first at 1392 °C, followed by austenite (FCC_A1) at 1272 °C. The ferrite begins to transform into the ordered B2 phase (BCC_B2) at 1181 °C, the equilibrium transformation is complete at 1158 °C, and the ferrite (BCC_A2) reappears at 646 °C, with the lower temperatures then favouring lower B2 contents. The austenite content also starts to decrease with decreasing temperatures and is close to zero at 458 °C. However, the austenite content is highest at 864 °C, as its content increases from its first appearance during solidification. The decrease in austenite at 864 °C is due to the precipitation of kappa carbides (KAPPA_E21), whose content increases with decreasing temperature.

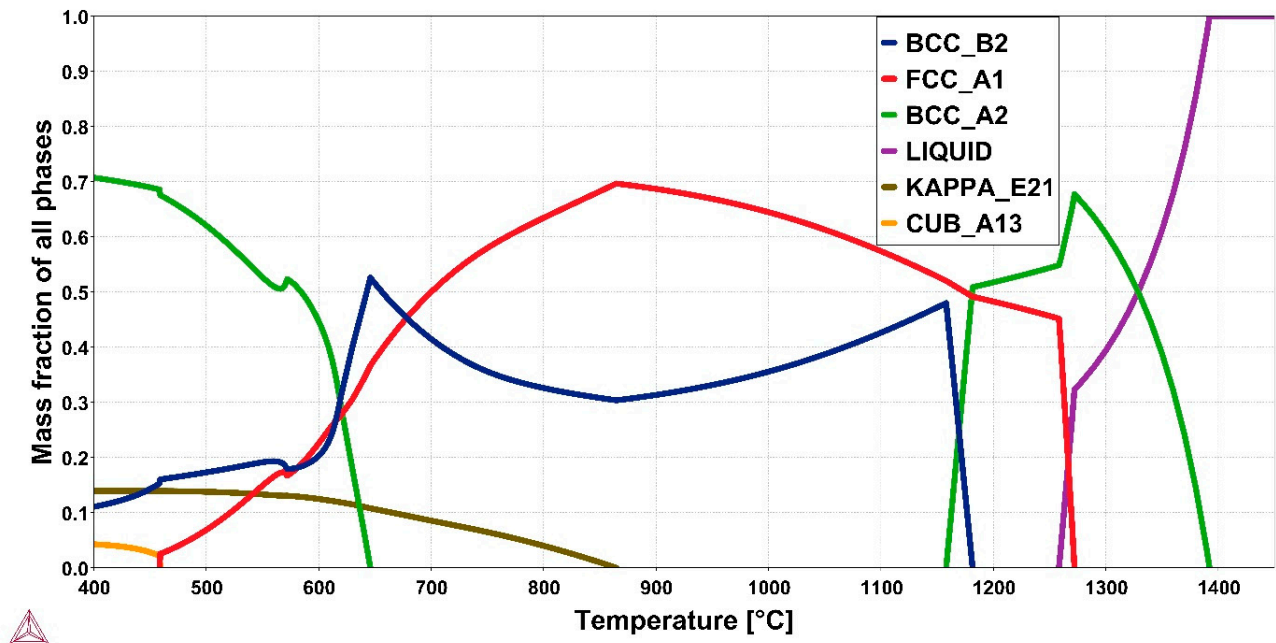


Figure 1. Thermo-Calc calculation of equilibrium amount of phase in Fe-Mn-Al-Ni-C at different temperatures.

3.2. Optical Microscopy

The etched samples showed different microstructures at different stages of the process. The microstructure of the as-cast sample consisted of γ -austenite phase with δ -ferrite islands. Some parts showed increased etching of the grain boundaries, an indication of possible precipitate formation. The microstructure of the as-cast sample is shown in Figure 2.

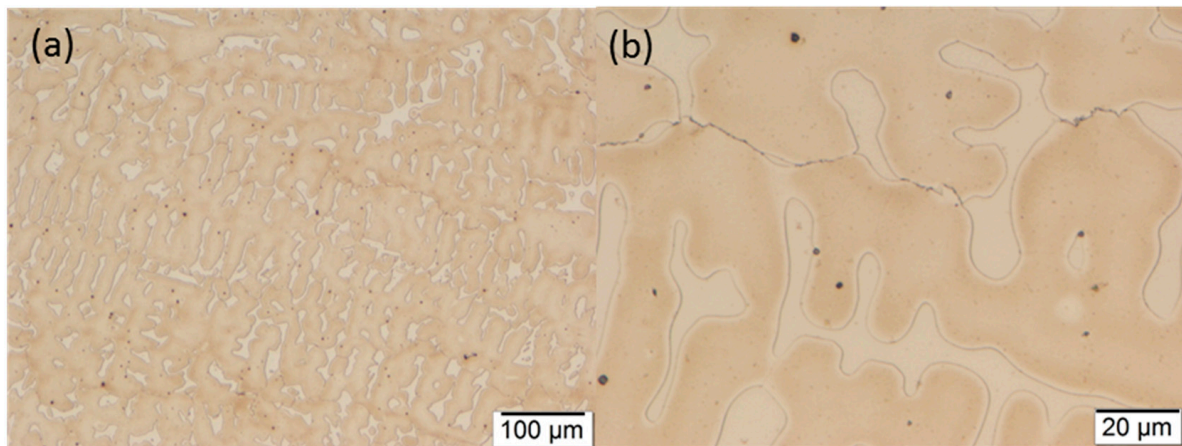


Figure 2. Optical microscopy of the as cast duplex microstructure, etched with 10% nital, ferrite—white, and austenite—brown (a) typical dendritic morphology, (b) somewhat enhanced etching of grain boundaries—possible precipitation.

Homogenization at 1200 °C and hot forging resulted in a slightly increased ferrite content (Figure 3), whereas slow cooling caused partial decomposition of the austenite, resulting in a more complex microstructure. The austenite grain boundaries are additionally enhanced, and the previously austenitic phase is now complex.

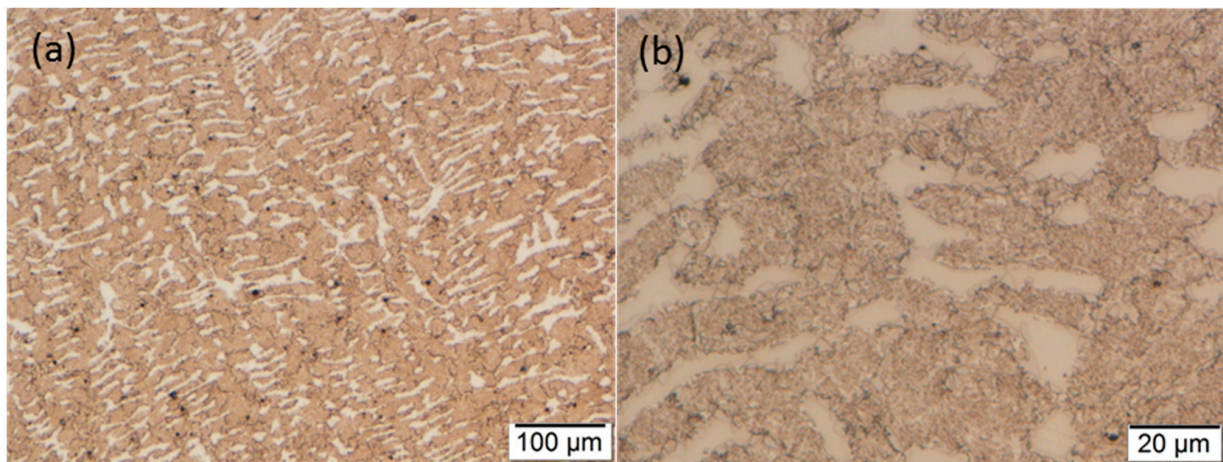


Figure 3. Optical microscopy of the forged complex microstructure, etched with 10% nital, ferrite—white, and austenite and carbides—darker brown; (a) the microstructure retained the dendritic morphology, (b) some enhanced grain boundaries—possible precipitation.

Solution annealing at 1200 °C and subsequent water quenching resulted in a simpler duplex microstructure of ferrite and austenite as shown in Figure 4. The microstructure underwent recrystallization during solution annealing as the dendritic structure was lost. The grain boundaries do not contain carbides, only ferrite and austenite are visible. The hot working direction is visible.

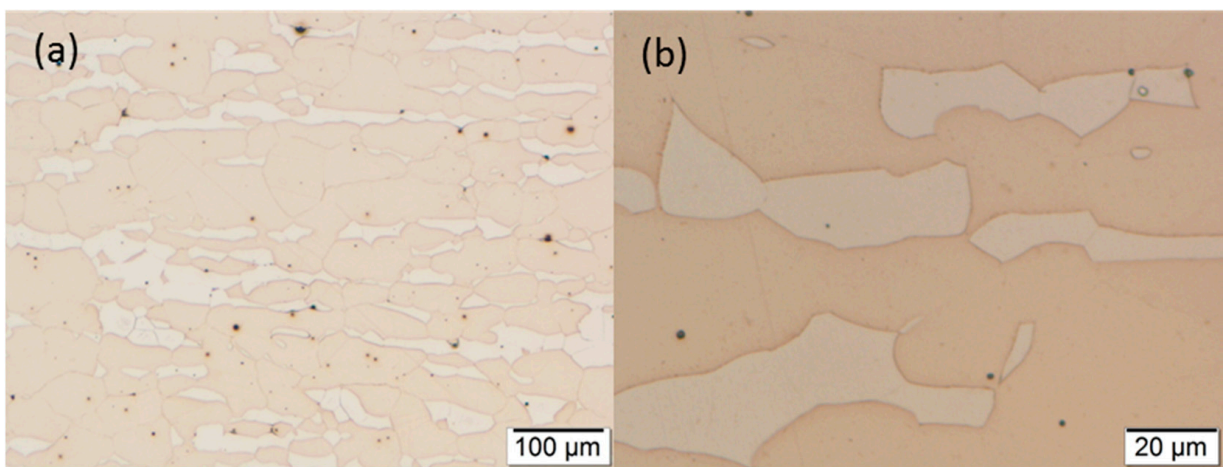


Figure 4. Optical microscopy of the as cast duplex microstructure, etched with 10% nital, ferrite—white, and austenite—brown; (a) the microstructure is elongated along the hot forging direction, but there is no visible deformation remaining in the crystal grains, indicating a full recrystallization, (b) magnified detail, there is no precipitation on the grain boundaries.

All other samples were, thus, solution annealed at 1200 °C, water quenched, and then isothermal annealed. The lowest isothermally annealed microstructure was at 350 °C, but the first visible change occurs at 550 °C.

Annealing at 350 °C resulted in a ferritic, austenitic microstructure, as shown in Figure 5. Isothermal annealing at 450 °C (Figure 6) gave the same result, however, both at 350 and 450 °C there is possible precipitation at grain boundaries.

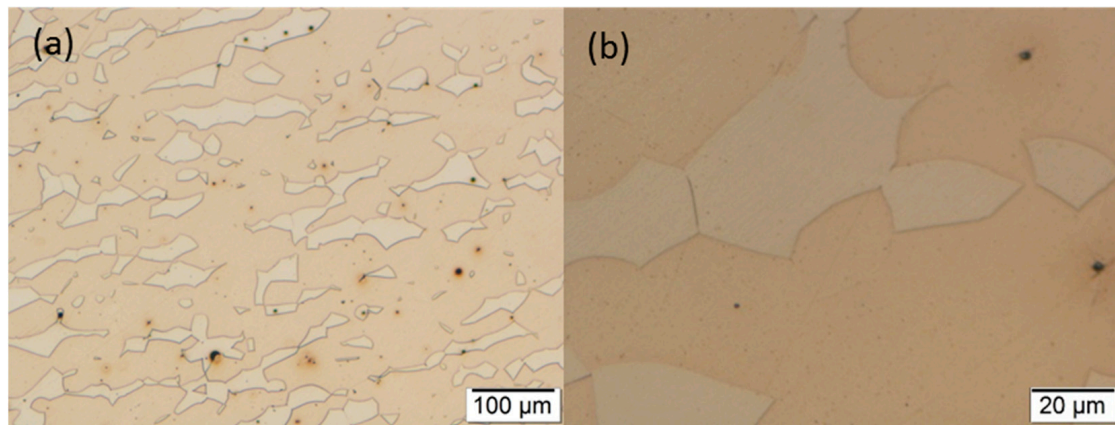


Figure 5. Optical microscopy of the sample that was isothermally annealed at 350 °C, etched with 10% nital, (a) ferrite—white, and austenite—brown, (b) magnified detail, there is possible precipitation on the grain boundaries.

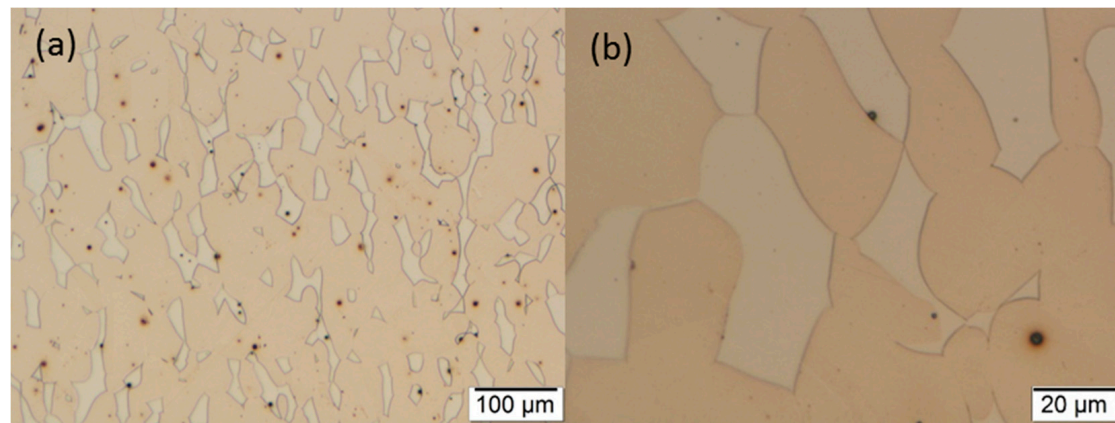


Figure 6. Optical microscopy of the sample that was isothermally annealed at 450 °C, etched with 10% nital, (a) ferrite—white, and austenite—brown, (b) magnified detail, there is possible precipitation on the grain boundaries.

Isothermal annealing at 550 °C resulted in a differently etched austenite phase. The etching caused a stronger coloration, as can be seen in Figure 7. The austenite was dark brown and purple in colour, a possible indication of precipitation. The grain boundaries are also more pronounced, indicating carbide precipitation. This occurs at all phase boundaries, ferrite and austenite.

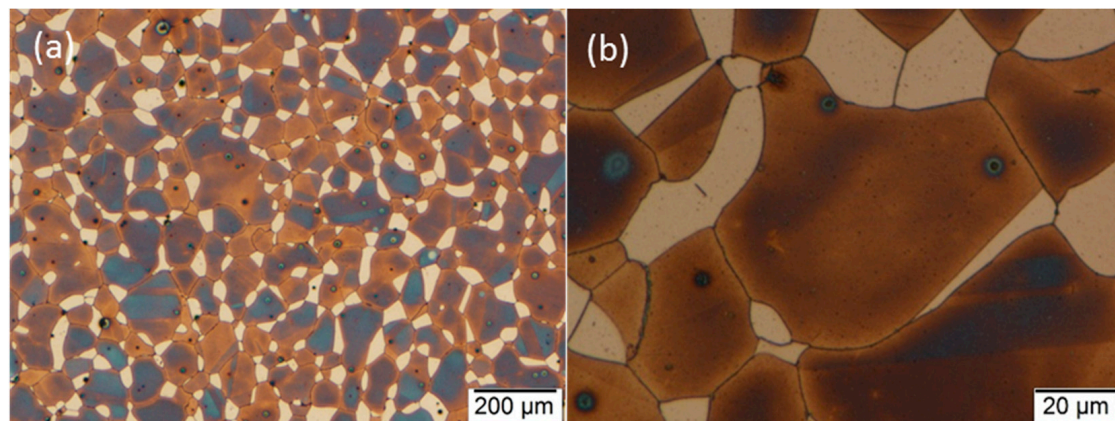


Figure 7. Optical microscopy of the sample that was isothermally annealed at 550 °C, etched with 10% nital, (a) ferrite—white, and austenite—dark brown and violet, (b) magnified detail, there is a strong precipitation on the grain boundaries, ferrite–ferrite, ferrite–austenite, and austenite–austenite.

A more dramatic change is seen with isothermal annealing at 650 °C. There is pronounced precipitation in the austenite phase, but surprisingly not at the ferrite–austenite grain boundary. The belt without precipitates is a few μm thick and appears white. The interior of the austenite is dark brown with even darker rod-like precipitates. The austenite–austenite grain boundaries do not limit the precipitation and are pronounced due to carbides, as seen in Figure 8. The ferrite phase appears to be free of precipitates. The ferrite–ferrite grain boundaries also appear to be free of precipitates.

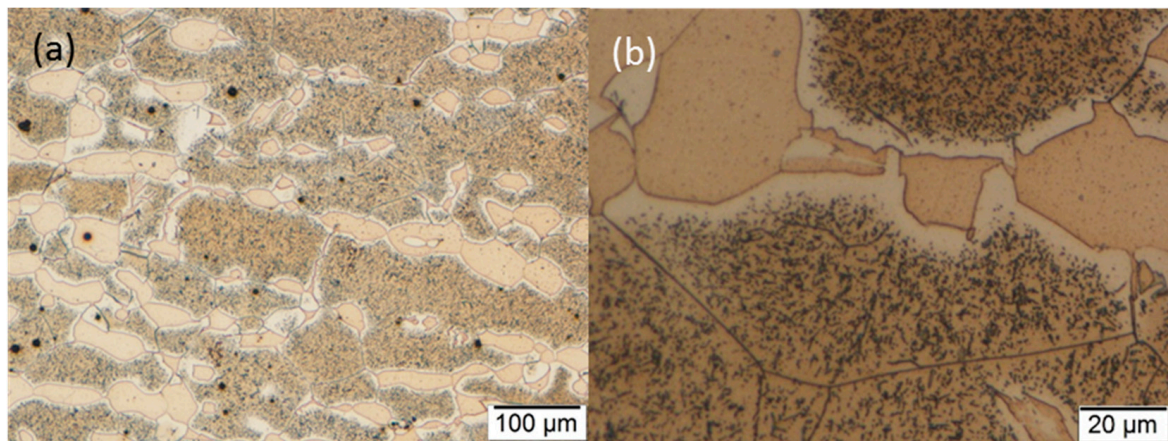


Figure 8. Optical microscopy of the sample that was isothermally annealed at 650 °C, etched with 10% nital, (a) ferrite—light brown, and austenite—dark brown with visible precipitation, (b) magnified detail, there is a strong precipitation on the ferrite–austenite and austenite–austenite grain boundaries.

At 750 °C, the grain boundaries thicken and clearly show a μm thick carbide layer. The austenite contains precipitates of about the same size as those at 650 °C, but they are less numerous. The main difference is the pronounced precipitation of carbides in the ferrite phase, as can be seen in Figure 9. Some of the carbides at the grain boundaries have started to become spherical.

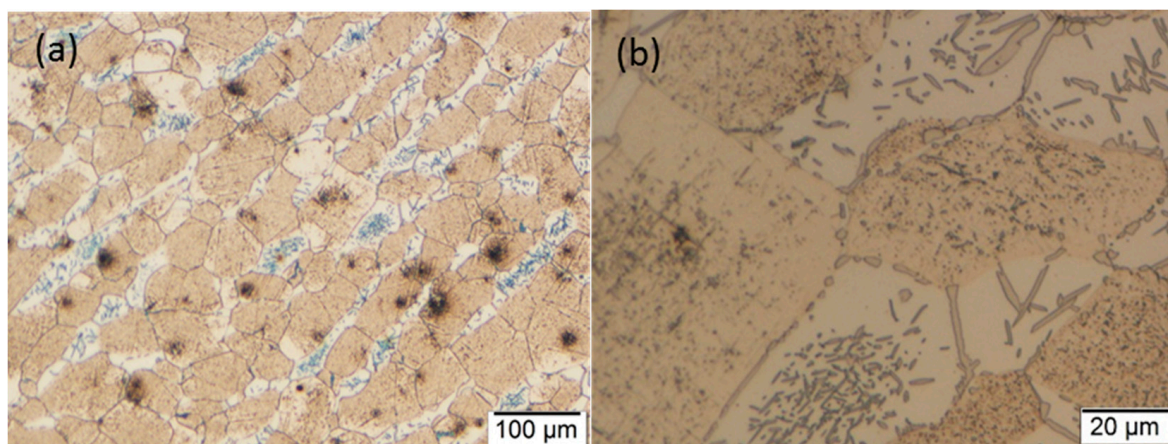


Figure 9. Optical microscopy of the sample that was isothermally annealed at 750 °C, etched with 10% nital, (a) ferrite—white with visible blueish carbide precipitates, and austenite—brown with visible precipitation, (b) magnified detail, there is a strong precipitation on the ferrite–ferrite and ferrite–austenite grain boundaries, the carbide film has begun to spheroidise.

The precipitation of carbides in ferrite is less pronounced at 850 °C, the carbides are coarser, but the precipitation in austenite is again more intense, the precipitates appearing in the form of twin boundaries, as can be seen in Figure 10.

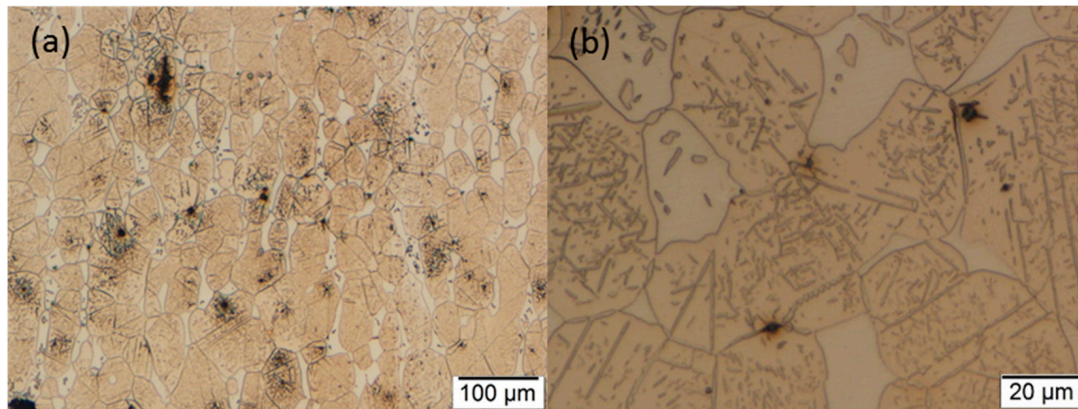


Figure 10. Optical microscopy of the sample that was isothermally annealed at 850 °C, etched with 10% nital, (a) ferrite—white with visible carbide precipitates, and austenite—brown with visible precipitation, (b) magnified detail, there is a strong precipitation in austenite, where the precipitates seem to have formed along the twin boundaries, the ferrite grains contain a few coarse carbides.

3.3. Scanning Electron Microscopy

A more detailed observation of the microstructures and precipitate phases was performed using scanning electron microscopy. Imaging as well as EDS and EBSD analyses were used to reveal details about the microstructure and precipitate phases.

Electron backscatter diffraction phase analysis confirmed that the as-cast sample consisted of FCC—austenite, with BCC—ferrite islands. The results are shown in Figure 11. No precipitate phases are visible in the microstructure at this scale. Figure 11c,d shows the elemental distribution maps obtained by EDS analysis of Al and Mn. The ferrite phase shows increased Al content and the austenite fraction shows increased Mn content, consistent with the formation of α and γ phases. No precipitates are visible in the EDS mapping, but higher magnification SE images shows a substructure in the austenite phase (Figure 12). The austenite substructure is formed by a spinodal transformation $\gamma \rightarrow \kappa + \gamma_0$ leading to nano-sized kappa carbides [18]. The ferrite–austenite grain boundary had a more pronounced etching effect.

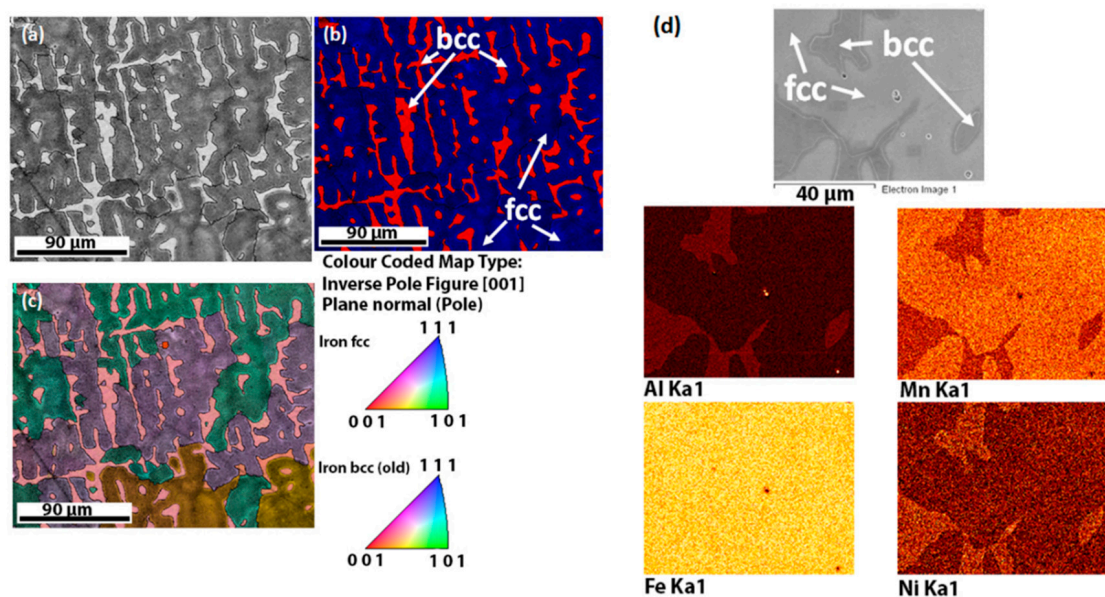


Figure 11. Microstructure of the as-cast sample, (a) BE (Backscattered electron) image, (b) EBSD (Electron Backscatter Diffraction) phase analysis (c) IPF-Z (Inverse Pole Figure–Z axis) analysis (d) EDS (Energy-dispersive X-ray spectroscopy) elemental mapping of Al, Mn, Fe, and Ni.

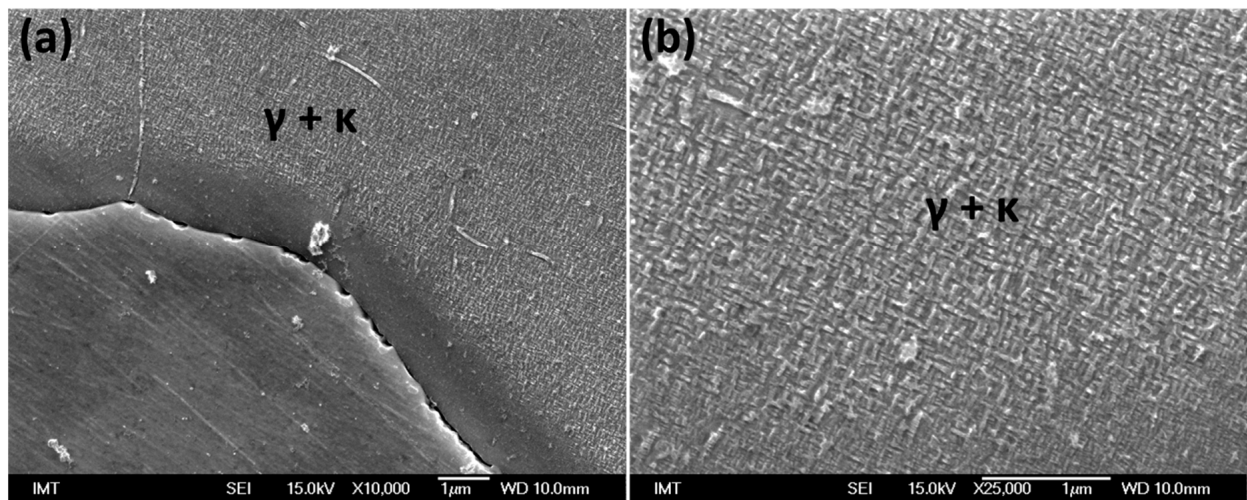


Figure 12. High magnification of the as-cast sample etched with 10% nital, (a) the austenite phase contains an ordering about a μm from the ferrite–austenite phase boundary, while the ferrite is precipitate free, (b) a more detailed image of the austenite containing ordering like precipitates.

Isothermal annealing changes the microstructure of the samples. Figure 13 shows backscattered electron images at lower magnification for samples annealed at 550 and 650 °C. The ferrite–austenite microstructure is maintained during annealing, although the ferrite and austenite content changes. Precipitation of the ordered B2 phase along the grain boundaries is evident at 550 °C. However, at 650 °C and above, precipitates were observed in the austenite, which were characterized in more detail using electron backscatter diffraction. The ordered B2 phase coarsens above 550 °C and can even be observed with an optical microscope.

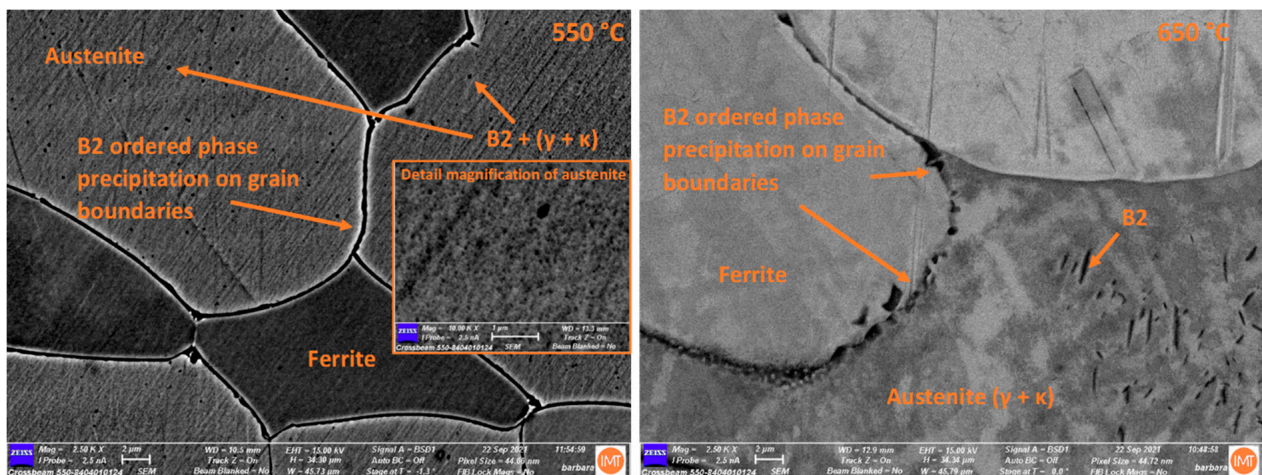


Figure 13. Backscattered electron images of the samples isothermally annealed at 550 and 650 °C.

At 750 °C, austenite and kappa-carbide phase precipitate in ferrite, similar to the sample annealed at 850 °C. However, the formation of kappa carbides in austenite is indicated by EBSD phase analysis, as shown in Figure 14, sample annealed at 850 °C. At 750 and especially 850 °C B2 ordered phase precipitates occur along the grain boundaries, on the austenite twins and within the austenite phase. The B2 ordered phase can be identified by its BCC crystal lattice, while the austenite has an FCC crystal lattice. In addition, the distinction between FCC austenite and perovskite kappa carbides is more difficult as both have similar features in EBSD analysis, but the difference can be seen in Figure 15.

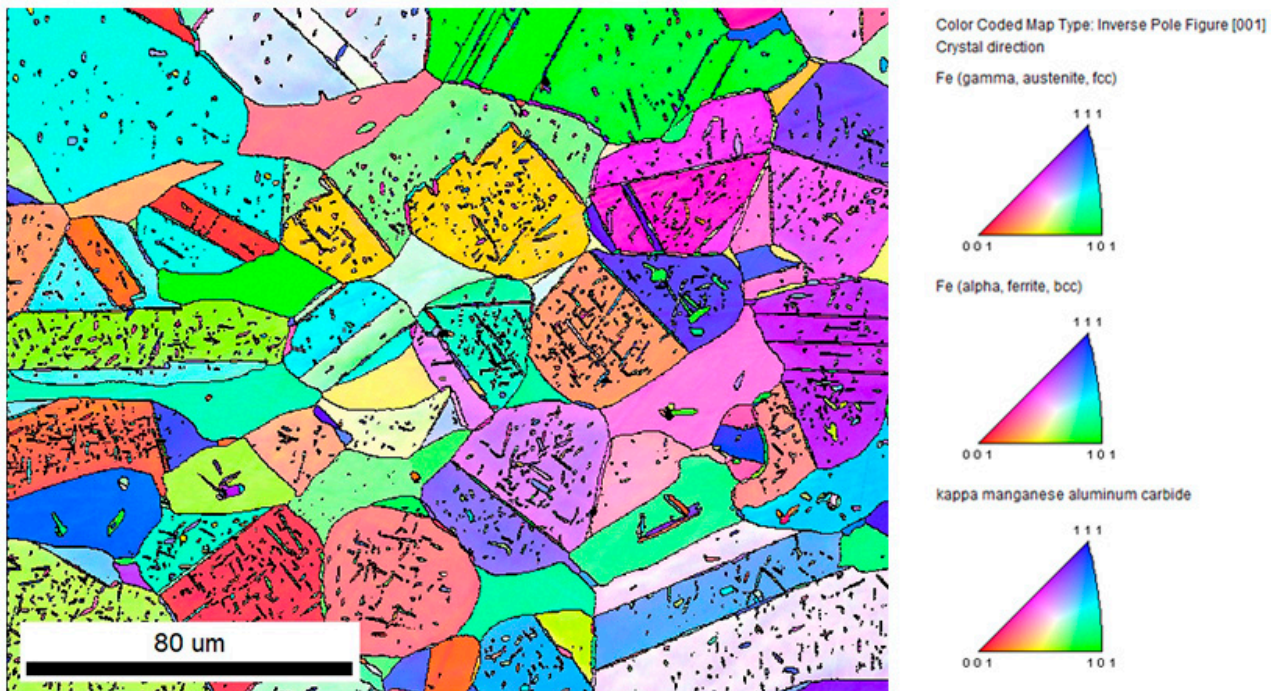


Figure 14. Electron backscattered diffraction analysis of a sample annealed at 850 °C showing different orientations of austenite with precipitated B2 ordered phase, along grain boundaries, on twins and intracrystalline.

Additional analysis of the orientation relationship between the austenite parent phase and the precipitate phase reveals a strong Kurdjumov–Sachs-like orientation relationship, as also indicated by the pole figure shown in Figure 15. In other words, the B2 ordered precipitates are coherent with parent austenite matrix, therefore, contributing to mechanical properties.

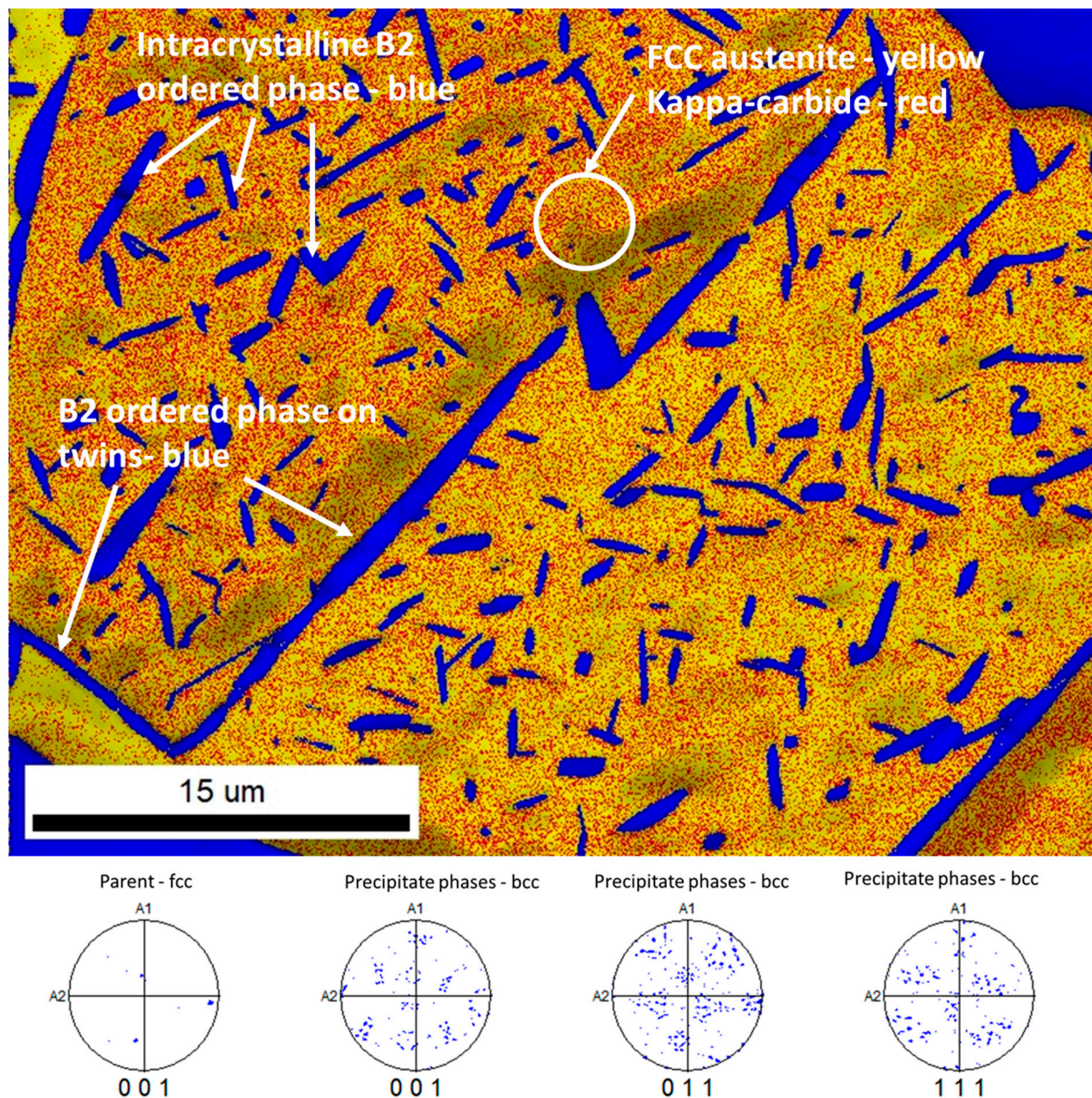


Figure 15. Results of EBSD analysis of the sample annealed at 850 °C, where the Kurdjumov–Sachs-like orientation relation proves the coherence of the FCC matrix and the BCC B2 ordered precipitates. Detailed analysis of the precipitates in austenite.

4. Conclusions

The synthesis of low-density steel Fe-Mn-Al-Ni-C has been studied. The basic microstructure of the steel is duplex ferritic and austenitic, cooling from high temperatures results in precipitation of kappa carbides and formation of B2 phases, as shown by the as-cast microstructure. Solution annealing at 1200 °C and water quenching are required to obtain a duplex microstructure. However, annealing below 864 °C leads to various kappa-carbide precipitates and the formation of B2 ordered phase. Moreover, austenite island formed in ferrite during isothermal annealing at 750 and 850 °C, coarse kappa carbides formed at temperatures above 650 °C, while nano-sized kappa precipitates were present at 550 °C. Annealing at 450 and 350 °C resulted in the formation of kappa carbides at grain boundaries, i.e., ferrite–austenite grain boundaries. The CALPHAD method has been successfully used to predict the microstructure of low-density Fe-Mn-Al-Ni-C steels.

Author Contributions: Conceptualization and writing, J.B., T.B. and B.Š.B.; original draft preparation, J.B., B.Š.B. and T.B.; methodology and formal analysis, J.B., B.Š.B. and T.B.; validation and formal analysis, J.B. and B.Š.B. All authors have read and agreed to the published version of the manuscript.

Funding: Funding was provided by the Slovenian Research Agency ARRS program P2-0050 (C).

Conflicts of Interest: The authors declare no conflict of interest.

References

1. Chen, S.; Rana, R.; Haldar, A.; Ray, R.K. Current state of Fe-Mn-Al-C low density steels. *Prog. Mater. Sci.* **2017**, *89*, 345–391. [[CrossRef](#)]
2. Howell, R.A.; Van Aken, D.C. A literature review of age hardening Fe-Mn-Al-C alloys. *Iron Steel Technol.* **2009**, *6*, 193–212.
3. Rana, R.; Lahaye, C.; Ray, R.K. Overview of Lightweight Ferrous Materials: Strategies and Promises. *JOM* **2014**, *66*, 1734–1746. [[CrossRef](#)]
4. Bartlett, L.; Van Aken, D. High Manganese and Aluminum Steels for the Military and Transportation Industry. *JOM* **2014**, *66*, 1770–1784. [[CrossRef](#)]
5. Rana, R. Low-Density Steels. *JOM* **2014**, *66*, 1730–1733. [[CrossRef](#)]
6. Frommeyer, G.; Brox, U. Microstructures and Mechanical Properties of High-Strength Fe-Mn-Al-C Light-Weight TRIPLEX Steels. *Steel Res. Int.* **2006**, *77*, 627–633. [[CrossRef](#)]
7. Kalashnikov, I.; Acselrad, O.; Shalkevich, A.; Pereira, L.C. Chemical composition optimization for austenitic steels of the Fe-Mn-Al-C system. *J. Mater. Eng. Perform.* **2000**, *9*, 597–602. [[CrossRef](#)]
8. Sutou, Y.; Kamiya, N.; Umino, R.; Ohnuma, L.; Ishida, K. High-strength Fe-20Mn-Al-C-based alloys with low density. *ISIJ Int.* **2010**, *50*, 893–899. [[CrossRef](#)]
9. Raabe, D.; Springer, H.; Gutierrez-Urrutia, I.; Roters, F.; Bausch, M.; Seol, J.B.; Koyama, M.; Choi, P.P.; Tsuzaki, K. Alloy Design, Combinatorial Synthesis, and Microstructure–Property Relations for Low-Density Fe-Mn-Al-C Austenitic Steels. *JOM* **2014**, *66*, 1845–1856. [[CrossRef](#)]
10. Jahn, M.T.; Chang, S.C.; Hsiao, Y.H. Transverse tensile and fatigue properties of Fe-Mn-Al-C alloys. *J. Mater. Sci. Lett.* **1989**, *8*, 723–724. [[CrossRef](#)]
11. Kayak, G.L. Fe-Mn-Al precipitation-hardening austenitic alloys. *Met. Sci. Heat Treat.* **1969**, *11*, 95–97. [[CrossRef](#)]
12. Zuazo, I.; Hallstedt, B.; Lindahl, B.; Selleby, M.; Soler, M.; Etienne, A.; Perlade, A.; Hasenpouth, D.; Cazottes, S.; Kleber, X.; et al. Low-Density Steels: Complex Metallurgy for Automotive Applications. *JOM* **2014**, *66*, 1747–1758. [[CrossRef](#)]
13. Chen, P.; Li, X.; Yi, H. The κ -carbides in low-density fe-mn-al-c steels: A review on their structure, precipitation and deformation mechanism. *Metals* **2020**, *10*, 1021. [[CrossRef](#)]
14. Cheng, W.C.; Song, Y.S.; Lin, Y.S.; Chen, K.F.; Pistorius, P.C. On the eutectoid reaction in a quaternary Fe-C-Mn-Al alloy: Austenite \rightarrow ferrite + kappa-carbide + M₂₃C₆ carbide. *Metall. Mater. Trans. A Phys. Metall. Mater. Sci.* **2014**, *45*, 1199–1216. [[CrossRef](#)]
15. Bartlett, L.N.; Van Aken, D.C.; Medvedeva, J.; Isheim, D.; Medvedeva, N.I.; Song, K. An atom probe study of kappa carbide precipitation and the effect of silicon addition. *Metall. Mater. Trans. A Phys. Metall. Mater. Sci.* **2014**, *45*, 2421–2435. [[CrossRef](#)]
16. Cheng, W.C.; Cheng, C.Y.; Hsu, C.W.; Laughlin, D.E. Phase transformation of the L12 phase to kappa-carbide after spinodal decomposition and ordering in an Fe-C-Mn-Al austenitic steel. *Mater. Sci. Eng. A* **2015**, *642*, 128–135. [[CrossRef](#)]
17. Rahnama, A.; Kotadia, H.; Clark, S.; Janik, V.; Sridhar, S. Nano-mechanical properties of Fe-Mn-Al-C lightweight steels. *Sci. Rep.* **2018**, *8*, 9065. [[CrossRef](#)] [[PubMed](#)]
18. Mapelli, C.; Barella, S.; Gruttadauria, A.; Mombelli, D.; Bizzozero, M.; Veys, X. γ Decomposition in Fe–Mn–Al–C lightweight steels. *J. Mater. Res. Technol.* **2020**, *9*, 4604–4616. [[CrossRef](#)]
19. Kimura, Y.; Handa, K.; Hayashi, K.; Mishima, Y. Microstructure control and ductility improvement of the two-phase γ -Fe/ κ -(Fe, Mn)₃AlC alloys in the Fe-Mn-Al-C quaternary system. *Intermetallics* **2004**, *12*, 607–617. [[CrossRef](#)]
20. Andersson, J.-O.; Thomas, H.; Lars, H.; Pingfang, S.; Bo, S. Thermo-Calc & DICTRA, computational tools for materials science. *Calphad* **2002**, *26*, 273–312. [[CrossRef](#)]
21. Thermo-Calc Software. *TCFE10: TCS Steel and Fe-Alloys Database*; Thermo-Calc AB: Stockholm, Sweden, 2019.